NSRRC-J04513 (2014)

ADVANCED FUNCTIONAL MATERIALS
www.afm-journal.de

www.MaterialsViews.com

High-Performance Nonvolatile Transistor Memories of Pentacence Using the Green Electrets of Sugar-based Block Copolymers and Their Supramolecules

Yu-Cheng Chiu, Issei Otsuka, Sami Halila, Redouane Borsali, and Wen-Chang Chen**

Reported here are the nonvolatile electrical characteristics of pentacene-based organic field-effect transistor (OFET) memory devices created from the green electrets of sugar-based block copolymer maltoheptaose-*block*-polystyrene (MH-*b*-PS), and their supramolecules with 1-aminopyrene (APy). The very hydrophilic and abundant-hydroxyl MH block is employed as a charge-trapping site, while the hydrophobic PS block serves as a matrix as well as a tunneling layer. The orientation of the MH nanodomains could be well controlled in the PS matrix with random spheres, vertical cylinders, and ordered horizontal cylinders via increasing solvent annealing time, leading to different electrical switching characteristics. The electron-trapping ability induced by the horizontal-cylinder MH is stronger than those of the random-sphere and vertical-cylinder structures, attributed to the effective contact area. The electrical memory window of the device is further improved via the supramolecules of hydrogen-bonding 1-aminopyrene to the MH moieties of MH-*b*-PS for enhancing the hole-trapping ability. The optimized device using the horizontal cylinders of the supramolecule electret exhibits the excellent memory characteristics of a wide memory window (52.7 V), retention time longer than 10^4 s with a high ON/OFF ratio of $>10^5$, and stable reversibility over 200 cycles. This study reveals a new approach to achieve a high-performance flash memory through the morphology control of sugar-based block copolymers and their supramolecules.

1. Introduction

Organic field-effect transistor (OFET) type memories have attracted extensive research interest due to the easily integrated structure and non-destructive reading in a single transistor.[1–14] In such devices, nano-floating gate dielectrics[15–20] or polymer electret[14,21–26] were employed widely as the charge trapping layer due to their effectiveness in creating the hysteresis behavior and modulating high- and low-conducting state using different applied gate-source bias. The morphology of nanoparticles[17–19] or trapping sites[27,28] and the strength of loaded electric field in the tunneling layer,[17,29] closely link to the trapping and retention capability for tuning the memory characteristics. For example, the large aggregated metallic particles would destroy the memory window[18] whereas the sparse distribution of nanoparticles could restrain the leakage of stored charges form their neighboring nanoparticles.[18,30] On the other hand, Kim et al.[17,18] disclosed that the electret of the nonpolar tunneling layer with the low-k materials, such as polystyrene ($\varepsilon \sim 2.6$), produced a larger built-in electric field and resulted in efficient charge transfer from the semiconductor to metallic nanoparticles.

Recently, hybrid electrets of block copolymer/metallic nanoparticles within an ordered periodic nanostructure have been used to integrate the tunneling layer and trapping elements. Leong *et al.* employed micellar poly(styrene-*b*-4-vinyl pyridine) hybridized with in situ synthesis of gold nanoparticles as the electret in a OFET memory; nevertheless, the low concentrations of nanoparticles led to a limited electrical memory window.[31] Watkins et al. successfully increased the nanoparticle composition up to 40 wt% in poly(styrene-*b*-2-vinyl pyridine) for achieving in the large memory window but still had the situation of charge loss in the data retention.[19] Amphiphilic block copolymers could self-assemble into ordered nanostructures[32–35] and the domain periodicity of microphase separation (d) scales as $d \sim aN^{2/3}\chi^{1/6}$ in the strong-segregation limit,[36] where N and χ are the degree of polymerization and Flory-Huggins interaction parameter. Thus, it is of interest in exploring block copolymers with small N and high χ values to minimize self-assembled feature sizes for improving the retention capability

Dr. Y.-C. Chiu, Prof. W.-C. Chen
Department of Chemical Engineering
National Taiwan University
Taipei 10617, Taiwan
E-mail: chenwc@ntu.edu.tw
Dr. I. Otsuka, Dr. S. Halila, Dr. R. Borsali
Centre de Recherches sur les Macromolécules Végétales (CERMAV, UPR-CNRS 5301)
affiliated with Grenoble Alpes University, member of Institut de Chimie Moléculaire de Grenoble (ICMG, FR-CNRS 2607) and Institut Carnot PolyNat, BP53
38041, Grenoble Cedex 9, France
E-mail: borsali@cermav.cnrs.fr

DOI: 10.1002/adfm.201304297

© 2014 WILEY-VCH Verlag GmbH & Co. KGaA, Weinheim

and adjusting in the threshold voltage shift. We have successfully prepared natural-synthetic green block copolymers of maltoheptaose-*block*-polystyrene and achieved well-organized patterns with sub-10 nm features.[39–41] Note that the χ value of MH-*b*-PS is 0.1 and much higher than that of PMMA-*b*-PS (0.01).[42] The very hydrophilic maltoheptaose block could exhibit the good trapping ability of mobile electrons and result in noticeable hysteresis in their transfer characteristics, similar to those reported in the literature.[18,26,37,38]

In this study, we report the electrical switching characteristics of pentacene based OFET memory devices using the electrets of sugar-based block copolymer thin films, maltoheptaose-*block*-polystyrene (MH-*b*-PS), and their supramolecules with 1-aminopyrene (MH(APy)-*b*-PS), as shown in **Figure 1**. The very hydrophilic and polyhydroxylated MH block served as charge-storage sites, while the hydrophobic and low-k PS block as a tunneling layer. This is the first example of using sugar based materials as the electrets of OFET memory devices, to the best of our knowledge. The orientation of the sub-10 nm MH cylinders surrounded by the PS matrix was controlled by varying annealing time using the solvent mixture of tetrahydrofuran/water (THF/H_2O = 1:1, w/w). The memory behaviors and retention capability were correlated with the morphology transformation of MH-*b*-PS. Furthermore, the supramolecular materials of MH(APy)-*b*-PS were prepared by hydrogen-bonding 1-aminopyrene with the MH moieties of MH-*b*-PS. The effects of the 1-aminopyrene (APy) composition on the hole-trapping capability of the MH-*b*-PS electrets were investigated. Our study demonstrated controlling the OFET memory characteristics using the nanostructures of the green electrets prepared from sugar based block copolymers and their supramolecules.

2. Results and Discussion

2.1. Structure Morphology of MH-*b*-PS Thin Films

The MH-*b*-PS thin film with the thickness of 43–45 nm was prepared by spin coating from the toluene solution, which is a poor solvent for the MH block, onto the Si(100) wafer with a 100-nm-thick SiO_2 and annealed by the mixture of THF/H_2O = 1:1. **Figure 2** shows the atomic force microscope (AFM) phase images of the MH-*b*-PS thin film as-cast and annealed by the THF/H_2O mixture for 8 h and 12 h, respectively, which exhibit poorly ordered spheres, packed dots, and fingerprint-like structures. The asymmetric structure of the MH-*b*-PS suggested that the observed morphology could consist of oriented domains of MH blocks (minor component) in a matrix of PS blocks (major component). The GISAXS data and the corresponding 2-D patterns of the three annealed films are shown in **Figure 3**. Combined with AFM image of Figure 2(a), the ring-like pattern of as-cast thin film observed in Figure 3(a) suggests the random sphere structure of the MH blocks, with the domain space of 10.4 nm, estimated by $d = 2\pi/q^*$ from q_y scans. The 8 h annealed film in Figure 3(b) suggests that MH cylinders are oriented vertically to the substrate with the spacing of 13.8 nm estimated from q_y scans. Note that the dots in the AFM image are probably the cross sections of the MH cylinders. For the 12 h annealed film of Figure 3(c), the clear diffraction spots with $1(q^*)$ are observed. In addition, the second-order peak can be seen in the q_y direction and high-ordered peaks in the q_z direction, suggesting that the MH cylinders with the domain spacing of 14.3 nm are well-orderly parallel to the substrate. The above results show that the thin-film morphologies of MH-*b*-PS change from random spheres, to ordered vertical and then well-ordered horizontal cylinders with increasing solvent annealing time. The morphological transformation from the vertical to horizontal cylinders is attributed to the change of the vapor composition in the sealed bottle. Since the evaporating speed of high-volatility THF is much faster than that of water, the chamber is filled with saturated THF vapor in the annealing period of 8 h. It results in the MH cylinders oriented perpendicular to the surface for minimize the interface between MH blocks and THF vapor. Note that the MH is miscible in H_2O and immiscible in THF. When the annealing time extends to 12 h, the H_2O vapor tends towards saturation and governs the MH blocks to migrate to the polymer-vapor interface, resulting in the MH cylinders horizontally to the surface. The MH-*b*-PS film with sphere, vertical-cylinder, and horizontal-cylinder morphologies are named as MHPS1, MHPS2, and MHPS3, respectively, in the following discussion on the OFET memory characteristics.

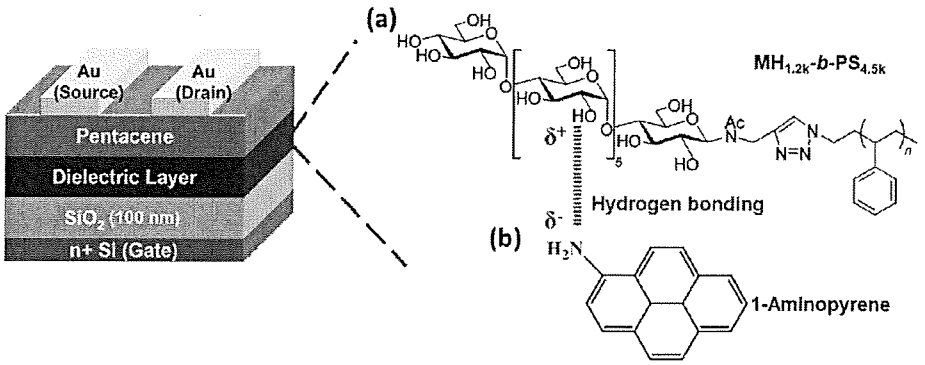

Figure 1. Schematic configuration of the pentacene-based OFET memory device and molecular structures of MH-*b*-PS and MH(APy)-*b*-PS supramolecules.

© 2014 WILEY-VCH Verlag GmbH & Co. KGaA, Weinheim

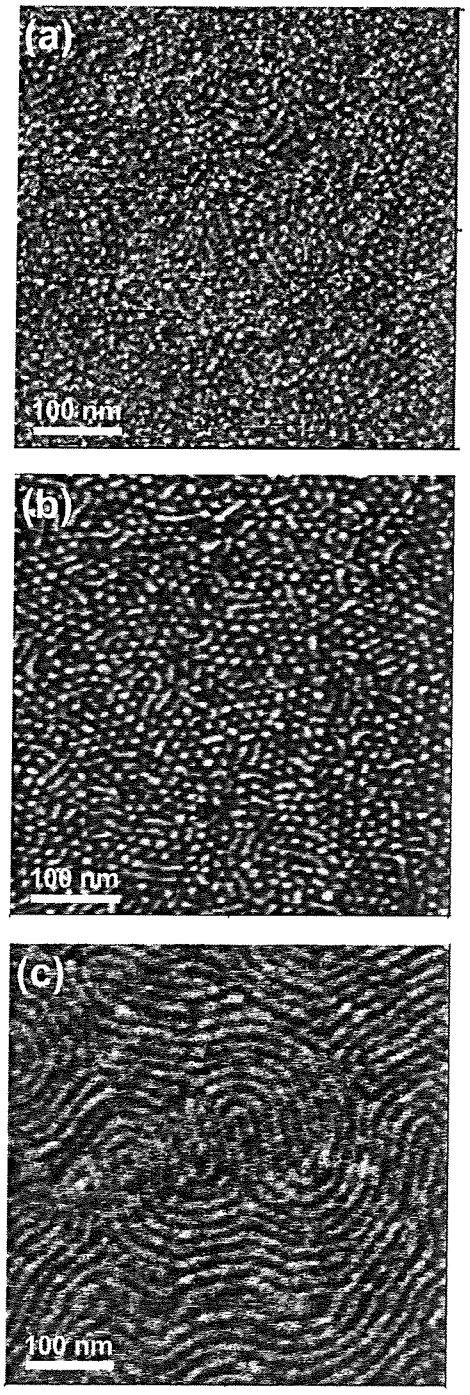

Figure 2. AFM phase images of the MS-*b*-PS film: (a) as-cast, (b) annealed 8 h, and (c) annealed 12 h.

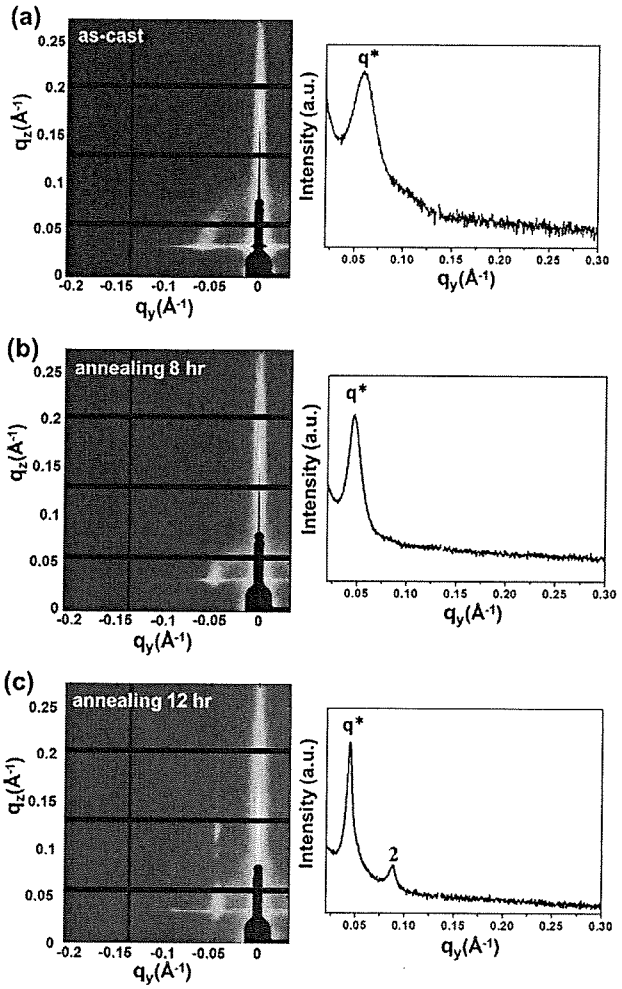

Figure 3. 2D GISAXS patterns and the q_y scans from the 2D-GISAXS patterns of MH-*b*-PS thin films annealed by the solvent mixture (H_2O/THF = 1/1) with various times.

2.2. OFET Memory Performance Using the MH-*b*-PS Electrets

The surface roughness of the MHPS1, MHPS2, and MHPS3 from the AFM images is below 0.3 nm, providing a good and defect-free surface for the growth of the pentacene semiconductor layer. The pentacene-based OFET memory device fabricated with a bottom-gate/top-contact configuration is shown in Figure 1, using the electret of MH-*b*-PS and compared to that of polystyrene (PS). The AFM images of pentacene grown on the polymer electrets are shown in Figure S1 (Supporting Information). The grain sizes of 50-nm pentacene grown on the surfaces of MHPS1, MHPS2, and MHPS3 are in the range of 200–300 nm, which is similar to that of the PS device. It suggests that the hydrophobic PS matrix of MH-*b*-PS maintains the similar surface energy to the polystyrene.

The dual-sweep curves on the initial transfer characteristics of the studied OFET memory devices are shown in **Figure 4** and the electrical characteristics are summarized in **Table 1**. All the measurements were studied in dark to prevent the light-induced charge transfer[43] or excitons.[14] The transfer curves exhibit a typical p-type accumulation mode with a good current modulation. The field-effect mobility (μ) measured in the saturation region of the devices using the polymer electrets of PS, MHPS1, MHPS2, and MHPS3 are 0.57, 0.59, 0.48, and 0.42 $cm^2V^{-1}s^{-1}$, respectively, with the I_{on}/I_{off} of ~10^8. The initial curves of the three OFET memory devices exhibit the hysteresis characteristic in Figure 4

© 2014 WILEY-VCH Verlag GmbH & Co. KGaA, Weinheim

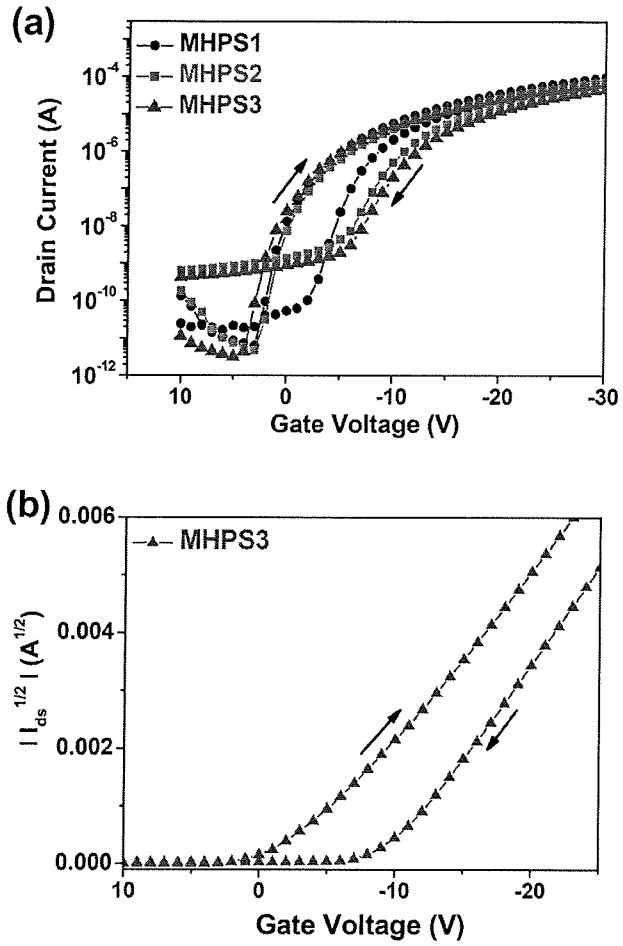

Figure 4. (a) Initial transfer characteristics of the devices using the electrets of MHPS1, MHPS2, and MHPS3 at $V_d = -30$ V. (b) The shifts in threshold voltage (hysteresis window) of the device using the MHPS3 electret.

with the threshold voltage (V_{th}) in the forward scans of –2.0 V(MHPS1), –2.3 V(MHPS2), and –1.7 V(MHPS3), respectively. For comparison, the OFET device incorporated with the PS electret shows no hysteresis between the forward and backward scans, with the corresponding V_{th} value of –6.8 V (Figure S2,Supporting Information), similar to that reported in the literature.[17,18,26] The MHPS1–3 electret based devices possess more positive V_{th} compared to that using the PS film, indicating the electron-trapping ability by the hydroxyl groups[44] of the MH blocks. The hysteresis windows defined by the difference of V_{th} between forward and backward curves (Figure 4b) are 4.1 V(MHPS1), 6.0 V(MHPS2), and 7.7 V(MHPS3), suggesting the strong dependence of the morphological transformations using the MH-*b*-PS electrets.

To investigate the electrical memory performance, the pentacene-based OFET memory devices were operated by applying the appropriate gate pulse to control the shifts of transfer curves. It leads to the high- (ON) and low-conductance (OFF) states at the zero gate bias condition ($V_g = 0$ V). Herein, the scans of drain current (I_d) versus V_g after the application of positive gate-source pulse (+50 V, 1 s) and negative one (–50 V, 1 s) are served as a "writing" and "erasing" processes, respectively. **Figure 5** shows the positive and negative shifts of the transfer curves (at a fixed drain voltage, V_d, of –30 V) of the OFET memory devices using the MHPS electrets, and the obtained memory characteristics are listed in Table 1. As shown in Figure 5(a), the PS-electret OFET for comparison shows the very small memory window (ΔV_{th}) of 4.8 V obtained from the difference between V_{th} of writing (–0.1 V) and erasing (–4.9 V). However, the transfer plots of MHPS1, MHPS2, and MHPS3 devices shown in Figure 5b–d are shifted to the more positive direction with V_{th} (writing) of 8.3, 7.0 and 13.8 V, respectively. In the following, the shifted transfer curves could be switched to the negative region close to their initial positions with V_{th} (erasing) of –8.5 V(MHPS1), –9.7 V(MHPS2), and –12.7 V(MHPS3) after applying an erasing operation with a reverse gate-bias to de-trap the electrons from the polarized MH block. Therefore, the memory windows of the MHPS1, MHPS2, and MHPS3 are 16.8 V, 16.7 V, and 26.5 V, respectively, which are significantly larger than that of the PS device due to the incorporated MH block with highly polar groups for trapping electrons. Also, the largest memory window observed in the MHPS3 device indicates that the charge-trapping ability induced by the horizontal-cylinder MH is stronger than those

Table 1. The electrical and memory performance of pentacene OFET devices using various dielectrics.

Electret	Morphology	μ_{ave} [$cm^2V^{-1}s^{-1}$]	$I_{On}/I_{Off,\ ave}$	$V_{th,\ ave}$ of writing [V]	$V_{th,\ ave}$ of erasing [V]	δV_{ave} [V]	Trapping density[a] Δn [cm^{-2}]
PS	Amorphous	0.57 ± 0.02	2.1×10^8	–0.1 ± 0.3	–4.9 ± 0.2	4.8	$6.40*10^{11}$
MHPS1[b]	Random sphere	0.59 ± 0.07	2.3×10^8	8.3 ± 0.8	–8.5 ± 0.7	16.8	$2.43*10^{12}$
MHPS2[b]	Vertical cylinder	0.48 ± 0.03	2.3×10^8	7.0 ± 1.6	–9.7 ± 0.6	16.7	$2.42*10^{12}$
MHPS3[b]	Horizontal cylinder	0.42 ± 0.01	$1.7*10^8$	13.8 ± 1.3	–12.7 ± 1.1	26.5	$3.84*10^{12}$
MHPy1[c]	Random sphere	0.33 ± 0.04	3.2×10^8	9.4 ± 0.7	–21.9 ± 1.5	31.3	$4.46*10^{12}$
MHPy2[c]	Horizontal cylinder	0.42 ± 0.03	4.7×10^8	13.2 ± 1.3	–25.6 ± 1.7	38.8	$5.52*10^{12}$
MHPy3[c]	Random sphere	0.32 ± 0.03	3.6×10^8	9.1 ± 0.9	–30.5 ± 2.0	39.6	$5.30*10^{12}$
MHPy4[c]	Horizontal cylinder	0.60 ± 0.06	3.2×10^8	14.3 ± 0.8	–38.4 ± 2.1	52.7	$7.05*10^{12}$

[a]The estimated charge trapping densities (Δn) is based on our previous reports.[23,24]; [b]MHPS1, MHPS2, and MHPS3 are the MH-b-PS film as cast, annealed for 8 h and 12 h, respectively.; [c](MHPy1, MHPy2) and (MHPy3, and MHPy4) contain 1 wt% and 5 wt% of 1-aminopyrene, respectively. Note that MHPy1and MHPy3 are as-cast films while MHPy2and MHPy4 are annealed for 12 h.

© 2014 WILEY-VCH Verlag GmbH & Co. KGaA, Weinheim

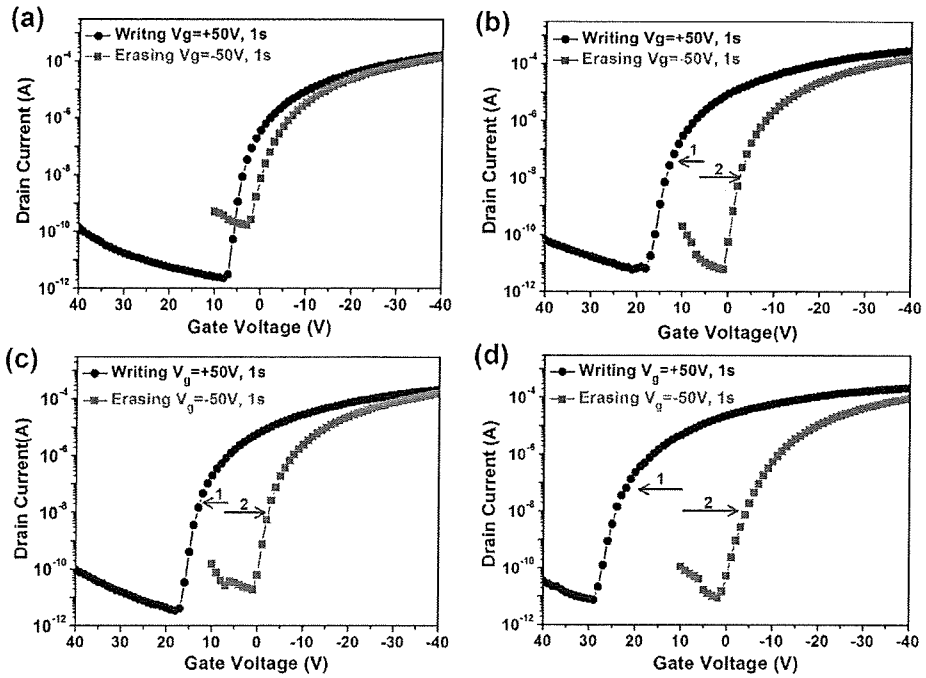

Figure 5. Transfer curves of the pentacene-based OFET memory device with different electrets, (a) PS, (b) MHPS1, (c) MHPS2 and (d) MHPS3. The drain current was measured at $V_d = -30$ V.

of random-sphere (MHPS1) and vertical-cylinder (MHPS2) structures. The larger contact area of the MH nanodomains of MHPS3 created in the interface between the semiconducting layer and polymer electret. Although the electron storage could be controlled by the MH structure, the MHPS devices show the poorly hole-trapping capability because the onset of the erasing curves maintains similarly at 0 V. In order to further enhance the memory window, the supramolecules of polyhydroxylated MH block with an electron-donating moiety, 1-aminopyrene (APy) are explored as the electret, through hydrogen bonding.

2.3. Transistor Memories Using the MH(APy)-*b*-PS Supramolecular Electrets

2.3.1. Morphology and Electrical Characterization

As shown in Figure 1(b), the APy molecules is attached to the hydroxyl groups of the MH block via hydrogen bonds to form supramolecular assemblies of MH(APy)-*b*-PS, effectively avoiding the strong aggregate from the π-π stacking between pyrene molecules. Two blending ratios of 1-wt% and 5-wt% APy to MH-*b*-PS(i.e., MH(1% APy)-*b*-PS and MH(5% APy)-*b*-PS) were prepared. The thin films of MH(APy)-*b*-PS with the thickness of 45 nm, were prepared from spin coating and following by solvent annealing, similar to that for MH-*b*-PS. The dielectric constant obtained from the frequency of 40 kHz for MH(1% APy)-*b*-PS and MH(5% APy)-*b*-PS films sandwiched by two metal electrodes are 3.13 and 2.94, which is lower than that of MH-*b*-PS (3.29). The decreasing tendency of dielectric constant with increasing APy composition suggests that the formation of hydrogen bonds in electrets reduces the amount of free hydroxyl groups in MH block, resulting in the suppressed polarized ability of MH-*b*-PS.[26]

Figure 6 shows the AFM and GISAXS result of the MH(1% APy)-*b*-PS thin films before and after 12 h solvent annealing. Note that phase transition is not observed upon addition of bipyridine in amylose-*block*-polystyrene system as already reported in our previous work.[40] Similar to the results of MH-*b*-PS thin film, the sphere-like morphologies are observed in the as-cast thin films of MH(1% APy)-*b*-PS and MH(5% APy)-*b*-PS (Figure S3, Supporting Information), with the domain spacing of 10.9 nm and 10.8 nm obtained from the first-order peaks in the q_y scans of GISAXS analyses (Figure 6(c) and Figure S3(c) of Supporting Information). After annealing in the vapor of THF/H_2O = 1:1 for 12 h, the morphologies of both films are converted to the long-range horizontal cylinders formed by MH(APy) surrounded by PS, as observed in Figure 6(b) and Figure S3(b). Also, no-large grains of APy phase-separated from MH-*b*-PS are shown in the figure, indicating the firmly hydrogen bonding between amino and hydroxyl groups. The GISAXS patterns of MH(1% APy)-*b*-PS and MH(5% APy)-*b*-PS show the estimated nanodomain periodicity of ~13.7 nm and ~13.9 nm. Also, the appearance of high-ordered peaks in the q_z direction reveals well-ordered horizontal cylinders similar to that of MH-*b*-PS after 12 h annealing. The MH-*b*-PS and MH(APy)-*b*-PS thin films present similar fingerprint-like structures after the same solvent-annealing time, due to the low composition of APy.

2.3.2. OFET Memory Performance using the MH(APy)-b-PS Electret

The electrets of random-sphere MH(1% APy)-*b*-PS, horizontal-cylinder MH(1% APy)-*b*-PS, random-sphere MH(5%

© 2014 WILEY-VCH Verlag GmbH & Co. KGaA, Weinheim

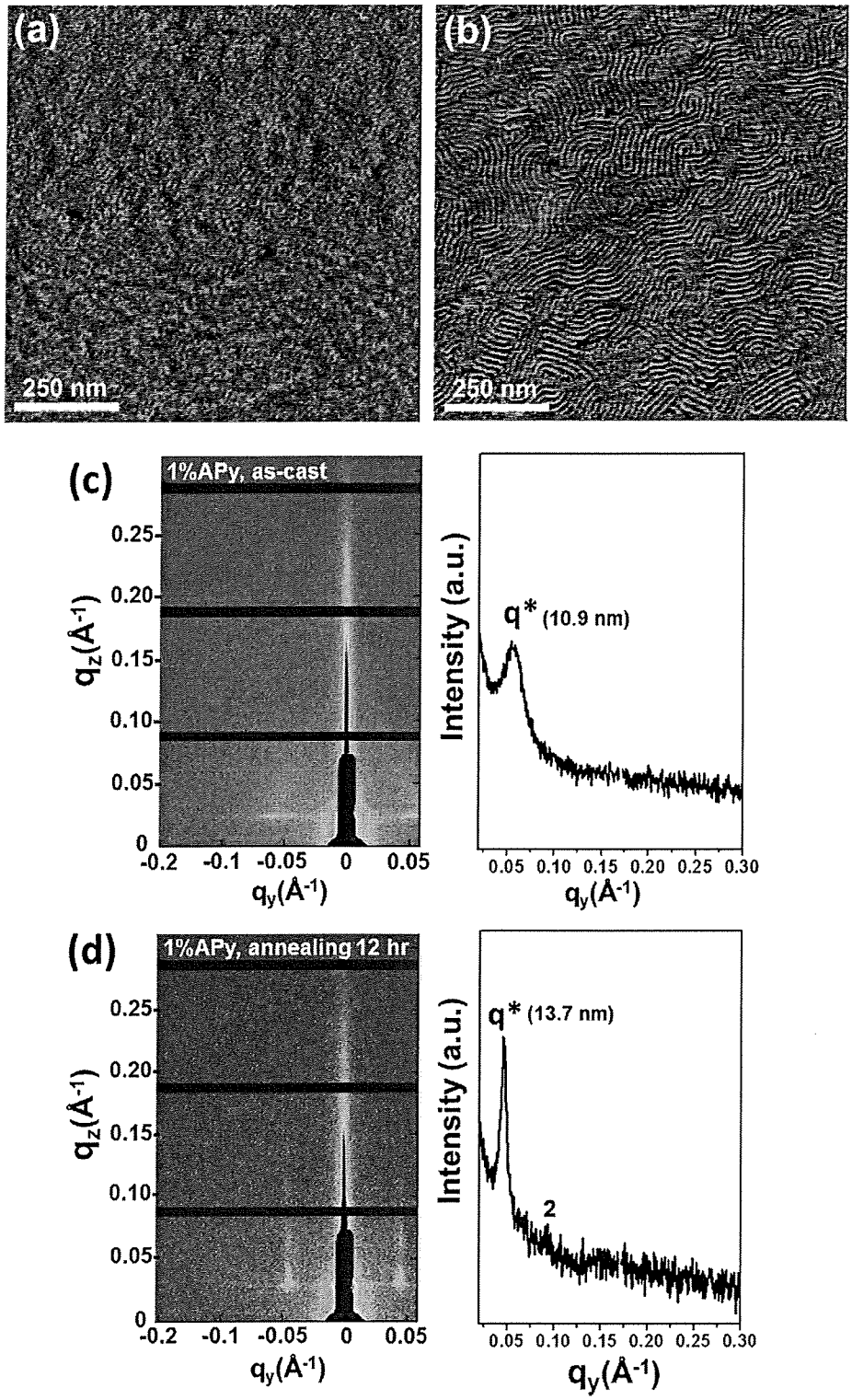

Figure 6. Structure characterization of the MH(1 wt% Apy)-*b*-PS thin film: AFM phase images of (a) as-cast thin film and (b) the film annealed by H_2O/THF (ratio: 1/1) for 12 h, and (c,d) 2D GISAXS patterns with their q_y scans spectra.

APy)-*b*-PS, and horizontal-cylinder MH(5% APy)-*b*-PS electrets are named as MHPy1, MHPy2, MHPy3, and MHPy4, respectively. **Figure 7** shows the transfer curves on the initial, writing, and erasing operations of the memory devices, and the electrical characteristics are listed in Table 1. The devices using the MH(APy)-*b*-PS electret also exhibits a high hole

© 2014 WILEY-VCH Verlag GmbH & Co. KGaA, Weinheim

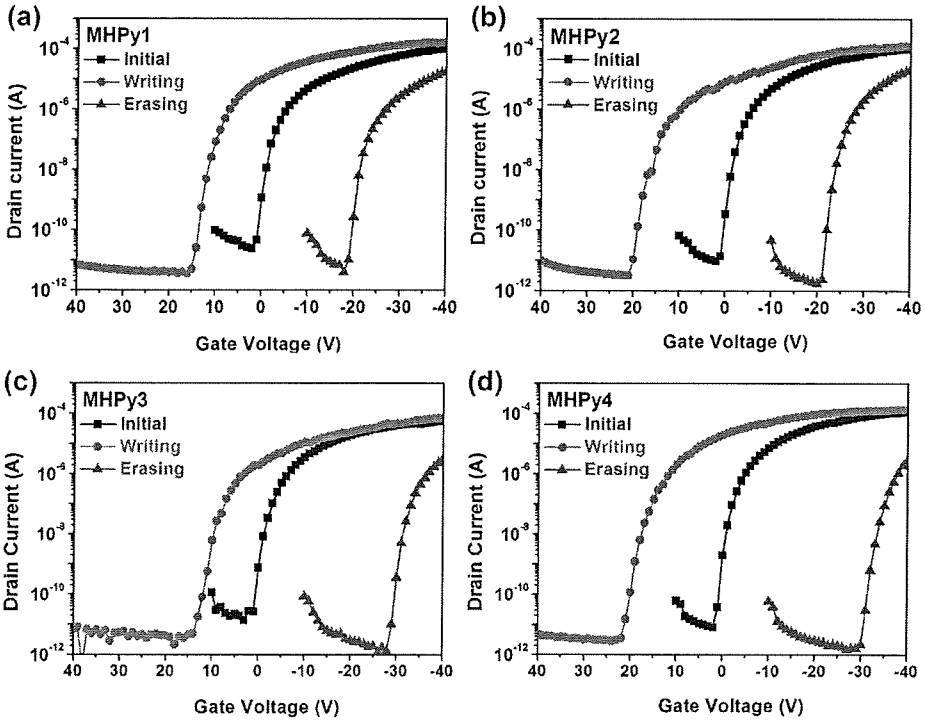

Figure 7. Transfer curves at $V_d = -30$ V of the OFET memory devices using the supramolecular thin films as the electrets. (a) MHPy1, (b) MHPy2, (c) MHPy3, and (d) MHPy4.

mobility of ~10^{-1} cm^2/Vs with high I_{on}/I_{off} current ratio over 10^8, similar to that using MHPS. For the memory devices using spherical MH(APy)-*b*-PS electrets (Figure 7(a,c)), the writing V_{th} of MHPy1 and MHPy3 devices are 9.4 V and 9.1 V, respectively, while the erasing V_{th} are −21.9 V and −30.5 V. The V_{th} of the writing curves is close to that of MHPS1 device (8.3 V), whereas the erasing V_{th} are shifted to a more negative region (−21.9 V for MHPy1 and −30.5 V for MHPy3), significantly larger than that of the MHPS1 device (−8.5 V, Figure 5b). It indicates that the grafted APy moiety into the electrets can effectively generate the hole-trapping capability due to their electron-donating nature. By contrast, the writing V_{th} of MHPy2 and MHPy4 devices are enhanced to 13.2 V and 14.3 V, which is larger than their films with the random sphere structure (MHPy1 and MHPy3) because of the larger interfacial area for the charge trapping using the horizontal cylinders. For the erasing process, the V_{th} are further switched to −25.6 V and −38.4 V for MHPy2 and MHPy4 devices. As a result, not only the hysteresis loops (Figure S4, Supporting Information) but also the memory window can be significantly improved from 16.8 V (MHPS1 device) to 52.7 V (MHPy4 device) with the high trapping density (Δn) of 7.05×10^{12} cm^{-2}.

2.4. Retention Characteristics and Reversibility

The retention capability of nonvolatile OFET memory devices was measured after the application of +50 V (ON state) and −50 V (OFF state) gate pulses for 1 s to investigate the carrier stability in the studied electrets. As shown in **Figure 8**(a), the stability extracted at the zero gate-source voltage for the ON and OFF memory states of the MHPS1, MHPS2, MHPS3, and MHPy2 based devices could be kept at least longer than 10^4 s without any current leakage. The separated sub-10 nm nanodomain of the MH moiety surrounded by tunneling the PS layer effectively results in the memory ratio (ON/OFF) over 10^6 throughout the monitor. In the devices using the horizontal-cylinder electrets, the ON-state current (5.9×10^{-6} A for MHPS3, 4.4×10^{-6} A for MHPy2) at 10^4 s is two to three times higher than that using the electrets of random sphere (1.6×10^{-6} A for MHPS1) or vertical-cylinder (1.8×10^{-6} A for MHPS2) structures. It indicates that the electret with the horizontal-cylinder MH block could induce a higher ON state current due to its larger shift in the writing process. However, the current value of the ON state using 5%-APy (MHPy4) electret dissipates slightly in the front period of 4000 s and then maintains the current stably. It indicates that the aminopyrene moiety significantly reduces the current leakage (Figure S5, Supporting Information).

The studied devices were tested by the cycle of the writing/reading/erasing/reading (WRER) operation to study their reproducible and reversible stability. The MHPS3 device could be retained over 100 cycles with the conductance change of ca. 3.6×10^3 (Figure S6 (Supporting Information)). However, the relative small ON/OFF value after 100-cycle measurement resulting from the high OFF current of ca. 3×10^{-10} A (Figure S6(b), Supporting Information) is attributed to that the onset voltage (+1.83 V) of the erasing curves (Figure 5(d)) is ahead of reading voltage (0V). This high OFF current occurred in the WRER test could be solved by grafting an electron-donating pyrene moiety onto the MH block, which effectively controls the onset of the erasing process at the negative bias and improve the switching stability further. As shown in

© 2014 WILEY-VCH Verlag GmbH & Co. KGaA, Weinheim

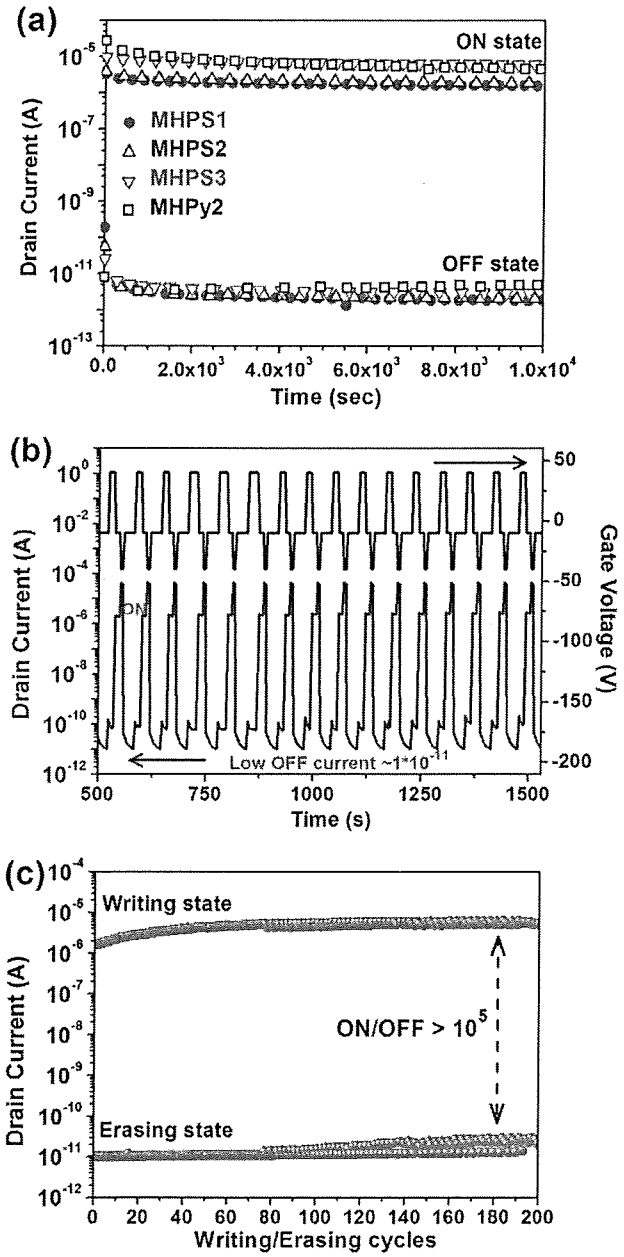

Figure 8. (a) Memory retention characteristics after the writing and erasing operation on the OFET memory devices (MHPS1, MHPS2, MHPS3, and MHPy2). The currents at ON and OFF states were read at $V_g = 0$V and $V_d = -30$ V. (b) The reversible switching on the ON- and OFF- states and (c) the endurance characteristics of the device using the MHPy2 electret.

Figure 8(b),(c), the MHPy2 device shows a stable switching behavior with the higher ON/OFF value of 4×10^5, which is much higher than that without the pyrene electret (MHPS3 device). Also, it exhibits an excellent reversibility between the writing and erasing states with a conductance change of ~10^5 being constantly maintained for over 200 cycles (Figure 8(c)). It suggests that the electron-donating aminopyrene can adjust the memory window by the negative shifts of the erasing curves, providing the relative low OFF current (1×10^{-11}) read out at a fixed voltage. To the best of our knowledge, the trapping density, memory window, retention capability and WRER properties of the OFET memory devices using sugar-based self-assembling supramolecules as electrets are comparable (or even better) to that of the state-of-the-art nano-floating gate and block copolymer-nanoparticle hybrid memory devices reported previously.[17–19,45] Also, such electret could have the advantage as environmentally friendly materials.

2.5. Origin of the Charge-Storage Behavior

The memory performance of the OFET memory based on MH-*b*-PS and MH(APy)-*b*-PS can be elucidated through the mechanism proposed in **Figure 9**. Via the solvent annealing, the orientation of the ordered MH nanodomains can be well-controlled in the PS matrix, including random spheres, vertical cylinders, and well-ordered horizontal cylinders. When applying the positive gate-source bias, the induced electron carriers can be trapped by the polarized hydroxyl groups[18,26] of the MH moieties in the MH-*b*-PS electret, leading to the positive shift of threshold voltage (Figure 9(a)). The shifted transfer curves recover to the threshold voltage similar to the initial state by the de-trapping process under a negative bias. Besides, the larger interface between pentacene and MH domains in the case of the horizontal cylinders triggers a bigger trapping density than the other two structures. Also, the PS matrix plays the role as the tunneling layer with the low-k property and thin thickness enhance the built-in field[17,18] to benefit the trapping process and stabilize the retention characteristics.

For the devices using MH(APy)-*b*-PS supramolecular electrets, the electron-trapping mechanism is same as the aforementioned writing process. When applying the negative gat-source bias, the threshold voltage of the erasing curve substantially shifts to a negative region via the injection of holes into the electron-donating pyrene moieties of MH(APy)-*b*-PS (Figure 9(b)). Since the memory window depends on the morphologies of supramolecules, the electret with the horizontal-cylinder structure exhibits the highest charge-storage capability. The above results not only demonstrate the high performance OFET memory could be achieved using the green electrets of sugar-based block polymers composed of the trapping and low-k tunneling moieties and their supramolecules.

3. Conclusions

We demonstrated that the sugar-based block copolymer thin films of maltoheptaose-*block*-polystyrene (MH-*b*-PS) and their supramolecules with 1-aminopyrene (APy) could serve as gate electrets for achieving a high-performance OFET memory device. The very hydrophilic polyhydroxylated MH block and the hydrophobic PS matrix act as the charge-trapping sites and tunneling layer, respectively. The different orientation of the MH cylinders surrounded by the PS matrix could be controlled by varying solvent-annealing time. The memory behavior and retention capability of the devices using the MH-*b*-PS electret

© 2014 WILEY-VCH Verlag GmbH & Co. KGaA, Weinheim

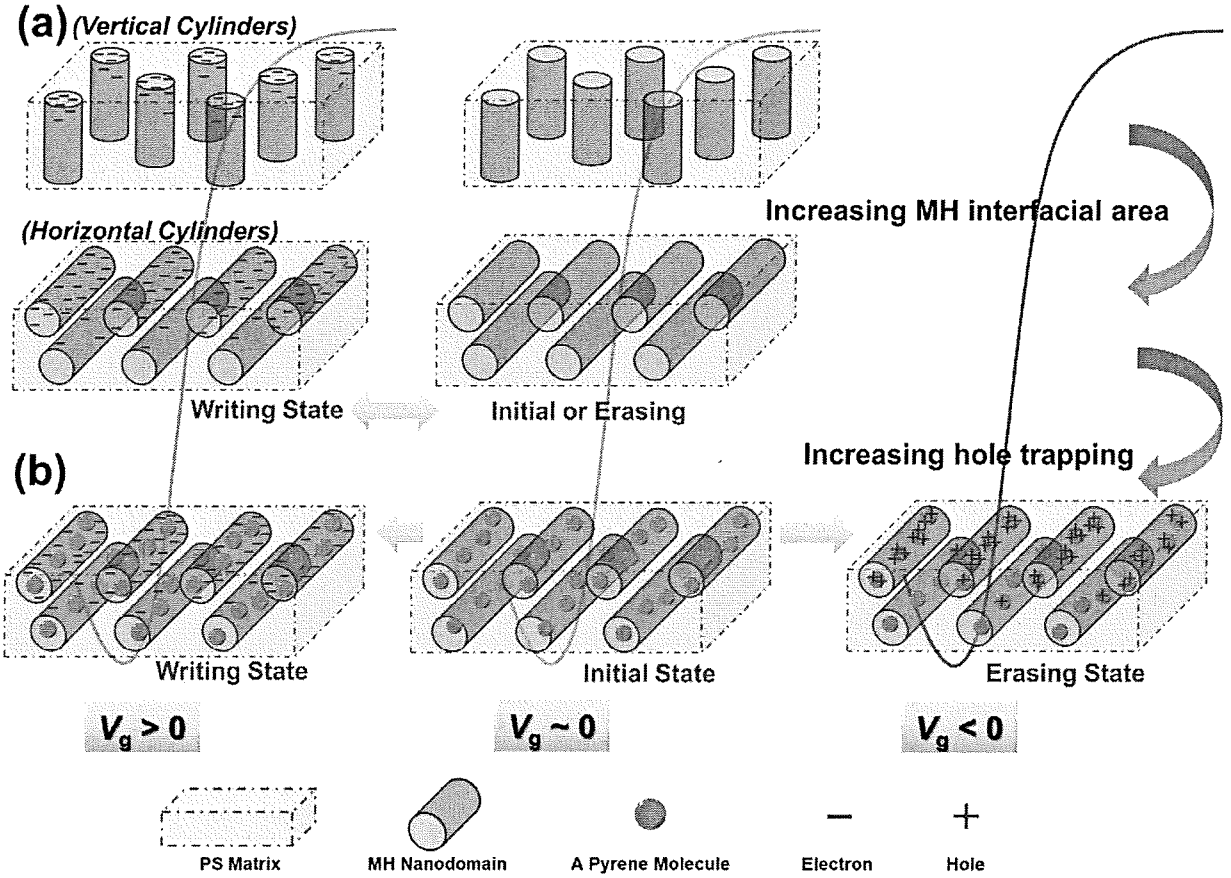

Figure 9. Illustration on tuning the memory characteristics of pentacene-based OFET memory under a positive and a negative bias using the following electrets: (a) MH-*b*-PS block copolymer, and (b) MH(APy)-*b*-PS supramolecule.

were significantly affected by the morphological transfer from random sphere, to vertical cylinders, and horizontal cylinders. Furthermore, the supramolecules were constructed by hydrogen-bonding APy to the MH moieties of a MH-*b*-PS. The hole-trapping capability of the device using the MH(APy) supramolecule electret with the horizontal cylinder structure was enhanced with increasing the APy composition, with the excellent memory characteristics of a wide memory window (52.7 V), long retention time over 10^4 s with high ON/OFF-current ratio (>10^5), and stable reversibility over 200 cycles without decay.

4. Experimental Section

Materials: The hybrid block copolymer, maltoheptaose-*block*-polystyrene (MH-*b*-PS) with $M_{n,MH}$ = 1200 g/mol and $M_{n,PS}$ = 4500 g/mol, was synthesized through copper-catalyzed azide-alkyne cyclodaddition (CuAAC) of propargyl-functionalized maltoheptaose with azido endfunctionalized polystyrene as reported by our group previously.[41] Pentacene (sublimed) was purchased from Luminescence Technology Corp (Taiwan) and 1-aminopyrene was purchased from Sigma-Aldrich (Missouri, USA). All of reagents or anhydrous were commercially available and used as received.

Thin Film Preparation, Device Fabrication and Measurement: The transistor-type memory device based on a 50-nm pentacene thin film was fabricated on the highly doped n-type Si(100) wafer with a 100-nm-thick SiO_2 treated with a solvent cleaning procedure and dried under a steam of nitrogen. A homogenous toluene solution of MH-*b*-PS with the concentration of 10 mg ml^{-1} was filtered through PTFE membrane and then spin-coated at 1000 rpm for 60 s onto the wafer substrate. The thickness of all studied electrets was controlled at about 43–45 nm. For solvent annealing, thin films were put in a tightly capped 2-liter glass bottle containing an uncapped 20-mL beaker filled with a mixture of 2.5 g of tetrahydrofuran (THF) and 2.5 g of water. After annealing, the polymer thin film was dried under vacuum at 40 °C overnight to remove residue solvents, and the pentacene was deposited with a growth rate of 0.4 nm s^{-1} at 10^{-7} Torr. Top-contact gold electrode (70 nm) was subsequently deposited by evaporating through a shadow mask with the channel length (L) and width (W) defined as 50 and 1000 μm, respectively.

All the measurements of the transistor memories were conducted using a Keithley 4200-SCS semiconductor parameter analyzer (Keithley Instruments Inc., Cleveland, OH, USA), with a Remote PreAmp (4200-PA) in a N_2-filled glove box at room temperature. Triaxial cables were connected into the probe station to minimize the background noise. The capacitance of the bilayer dielectrics was measured at 40 kHz on metal-insulator-metal (MIM) structures using a Keithley 4200-SCS instrument equipped with a digital capacitance meter (model 4210-CVU), similar to the method we reported previously.[24] The relations between capacitance (C_{tot}) of the device, SiO_2 layer (C_{SiO2}), polymer electret (C_{poly}) and polymer dielectric constant (ε) are defined and calculated as our previous reports.[22–24] The carrier mobility (μ) and

© 2014 WILEY-VCH Verlag GmbH & Co. KGaA, Weinheim

threshold voltage (V_{th}) were estimated from slope and intercept of the linear plot of the square root of drain-to-source current ($I_{ds}^{1/2}$) versus the gate voltage (V_g) by the following equation in the saturation regime:

$$I_{ds} = \frac{WC_{tot}\mu}{2L}(V_g - V_{th})^2 \quad (1)$$

where C_{tot} is the capacitance per unit area of total dielectric layer and V_{th} is threshold voltage.

Characterization: The surface structure of pentacene or polymer film was obtained with a Nanoscope 3D controller atomic force micrograph (AFM, Digital Instruments) operated in the tapping mode at room temperature. Grazing incidence small-angle X-ray scattering (GISAXS) was conducted on beamline BL23A1 in the National SynchrotronRadiation Research Center (NSRRC), Taiwan.[46] A monochromatic beam of $\lambda = 1.240$ Å was used and the incident angle was 0.15°. The scattering patterns were collected on a Mar-CCD with a diameter of 165 mm. The scattering intensity profiles were reported as the plots of the scattering intensity I vs. the scattering vector q, where $q = (4\pi/\lambda)\sin(\theta/2)$ and θ is the scattering angle.

Supporting Information

Supporting Information is available from the Wiley Online Library or from the author.

Acknowledgements

The authors thank the financial support of this work from National Science Council (NSC), Taiwan. R. B. thanks "Institut Carnot PolyNat" and ANR, Labex Arcane ANR-11-LABX-0003–01, for the financial support.

Received: December 28, 2013
Revised: February 18, 2014
Published online: April 1, 2014

[1] S. Möller, C. Perlov, W. Jackson, C. Taussig, S. R. Forrest, *Nature* **2003**, *426*, 166.
[2] Q. D. Ling, D. J. Liaw, C. Zhu, D. S. H. Chan, E. T Kang, K. G. Neoh, *Prog. Polym. Sci.* **2008**, *33*, 917.
[3] J. Ouyang, C.-W. Chu, C. R. Szmanda, L. Ma, Y. Yang, *Nat. Mater.* **2004**, *3*, 918.
[4] P. Heremans, G. H. Gelinck, R. M. Muller, K. J. Baeg, D. Y. Kim, Y. Y. Noh, *Chem. Mater.* **2011**, *23*, 341.
[5] C. L. Liu, W. C. Chen, *Polym. Chem.* **2011**, *2*, 2169.
[6] N. G. Kang, B. Cho, B. G. Kang, S. Song, T. Lee, J. S. Lee, *Adv. Mater.* **2012**, *24*, 385.
[7] R. C. G. Naber, K. Asadi, P. W. M. Blom, D. M. de Leeuw, B. de Boer, *Adv. Mater.* **2010**, *22*, 933.
[8] W. P. Lin, S. J. Liu, T. Gong, Q. Zhao, W. Huang, *Adv. Mater.* **2013**, DOI: 10.1002/adma.201302637
[9] R. C. G. Naber, C. Tanase, P. W. M. Blom, G. H. Gelinck, A. W. Marsman, F. J. Touwslager, S. Setayesh, D. M. D. Leeuw, *Nat. Mater.* **2005**, *4*, 243.
[10] K.-J. Baeg, Y.-Y. Noh, J. Ghim, S.-J. Kang, H. Lee, D.-Y. Kim, *Adv. Mater.* **2006**, *18*, 3179.
[11] C. A. Di, F. Zhang, D. Zhu, *Adv. Mater.* **2013**, *25*, 313.
[12] S.-T. Han, Y. Zhou, Z.-X. Xu, L.-B. Huang, X.-B. Yang, V. A. L. Roy, *Adv. Mater.* **2012**, *24*, 3556.
[13] S. J. Kim, J. S. Lee, *Nano Lett.* **2010**, *10*, 2884.
[14] Y. Guo, C. A. Di, S. Ye, X. Sun, J. Zheng, Y. Wen, W. Wu, G. Yu, Y. Liu, *Adv. Mater.* **2009**, *21*, 1954.
[15] T. Sekitani, T. Yokota, U. Zschieschang, H. Klauk, S. Bauer, K. Takeuchi, M. Takamiya, T. Sakurai, T. Someya, *Science* **2009**, *326*, 1516.
[16] R. Schroeder, L. A. Majewski, M. Grell, *Adv. Mater.* **2004**, *16*, 633.
[17] K.-J. Baeg, Y.-Y. Noh, H. Sirringhaus, D.-Y. Kim, *Adv. Funct. Mater.* **2010**, *20*, 224.
[18] M. Kang, K.-J. Baeg, D. Khim, Y.-Y. Noh, D.-Y. Kim, *Adv. Funct. Mater.* **2013**, *23*, 3503.
[19] Q. Wei, Y. Lin, E. R. Anderson, A. L. Briseno, S. P. Gido, J. J. Watkins, *ACS Nano* **2012**, *6*, 1188.
[20] S.-T. Han, Y. Zhou, C. Wang, L. He, W. Zhang, V. A. L. Roy, *Adv. Mater.* **2013**, *25*, 872.
[21] K. J. Baeg, Y. Y. Noh, J. Ghim, B. Lim, D. Y. Kim, *Adv. Funct. Mater.* **2008**, *18*, 3678.
[22] J. C. Hsu, W. Y. Lee, H. C. Wu, K. Sugiyama, A. Hirao, W. C. Chen, *J. Mater. Chem.* **2012**, *22*, 5820.
[23] Y. H. Chou, N. H. You, T. Kurosawa, W. Y. Lee, T. Higashihara, M. Ueda, W. C. Chen, *Macromolecules* **2012**, *45*, 6946.
[24] Y. C. Chiu, C. L. Liu, W. Y. Lee, Y. Chen, T. Kakuchi, W. C. Chen, *NPG Asia Mater.* **2013**, *5*, e35.
[25] W. Wu, H. Zhang, Y. Wang, S. Ye, Y. Guo, C. Di, G. Yu, D. Zhu, Y. Liu, *Adv. Funct. Mater.* **2008**, *18*, 2593.
[26] T.-D. Tsai, J.-W. Chang, T.-C. Wen, T.-F. Guo, *Adv. Funct. Mater.* **2013**, *23*, 4206.
[27] M. Burkhardt, A. Jedaa, M. Novak, A. Ebel, K. Voitchovsky, F. Stellacci, A. Hirsch, M. Halik, *Adv. Mater.* **2010**, *22*, 2525.
[28] Z. Z. Du, W. Li, W. Ai, Q. Tai, L. H. Xie, Y. Cao, J. Q. Liu, M. D. Yi, H. F. Ling, Z. H Li, W. Huang, *RSC Adv.* **2013**, *3*, 25788.
[29] Y. C. Chiu, T. Y. Chen, C. C. Chueh, H. Y. Chang, K. Sugiyama, Y. J. Sheng, A. Hirao, W. C. Chen, *J. Mater. Chem. C* **2014**, *2*, 1436.
[30] S.-T. Han, Y. Zhou, Z.-X. Xu, V. A. L. Roy, T. F. Hung, *J. Mater. Chem.* **2011**, *21*, 14575.
[31] W. L. Leong, P. S. Lee, A. Lohani, Y. M. Lam, T. Chen, S. Zhang, A. Dodabalapur, S. G. Mhaisalkar, *Adv. Mater.* **2008**, *20*, 2325.
[32] F. S. Bates, G. H. Fredrickson, *Phys. Today* **1999**, *52*, 32.
[33] M. Changez, N. G. Ng, C. H. Lee, J. S. Lee, *Small* **2010**, *6*, 63.
[34] W. Hamley, *The Physics of Block Copolymers*, Oxford University Press, New York **1998**.
[35] W. L. Leong, N. Mathews, S. Mhaisalkar, Y. M. Lam, T. Chen, P. S. Lee, *J. Mater. Chem.* **2009**, *19*, 7354.
[36] F. S. Bates, G. H. Fredrickson, *Annu. Rev. Phys. Chem.* **1990**, *41*, 525.
[37] M. Egginger, M. I. Vladu, R. Schwödiauer, A. Tanda, I. Frischauf, S. Bauer, N. S. Sariciftci, *Adv. Mater.* **2008**, *20*, 1018.
[38] Th. B. Singh, N. Marjanovi , G. J. Matt, N. S. Sariciftci, R. Schwödiauer, *Appl. Phys. Lett.* **2004**, *85*, 5409.
[39] J. Cushen, I. Otsuka, C. Bates, S. Halila, S. Fort, C. Rochas, J. Easley, E. Rausch, A. Thio, R.Borsali, G.Willson, C. Ellison, *ACS Nano* **2012**, *6*, 3424.
[40] K. Aissou, I. Otsuka, C. Rochas, S. Fort, S. Halila, R. Borsali, *Langmuir* **2011**, *27*, 4098.
[41] Otsuka, S. Tallegas, Y. Sakai, C. Rochas, S. Halila, S. Fort, A. Bsiesy, T. Baron, R. Borsali, *Nanoscale* **2013**, *5*, 2637.
[42] S. Tallegas, C. Rochas, R. Borsali, unpublished.
[43] B. Park, P. Paoprasert, I. In, J. Zwickey, P. E. Colavita, R. J. Hamers, P. Gopalan, P. G. Evans, *Adv. Mater.* **2007**, *19*, 4353.
[44] K.-J. Baeg, A. Facchetti, Y.-Y. Noh, *J. Mater. Chem.* **2012**, *22*, 21138.
[45] C. M. Chen, C. M. Liu, K. H. Wei, U. S. Jeng, C. H. Su, *J. Mater. Chem.* **2012**, *22*, 454.
[46] U. S. Jeng, C. H. Su, C. J. Su, K. F. Liao, W. T. Chuang, Y. H. Lai, J. W. Chang, Y. J. Chen, Y. S. Huang, M. T. Lee, K. L. Yu, J. M. Lin, D. G. Liu, C. F. Chang, C. Y. Liu, C. H. Chang, K. S. Liang, *J. Appl. Crystallogr* **2010**, *43*, 110.

© 2014 WILEY-VCH Verlag GmbH & Co. KGaA, Weinheim